



Plains CO<sub>2</sub> Reduction (PCOR) Partnership  
Energy & Environmental Research Center (EERC)

# PETROPHYSICAL EVALUATION OF CORE FROM THE AQUISTORE CO<sub>2</sub> INJECTION SITE

## Plains CO<sub>2</sub> Reduction (PCOR) Partnership Value-Added Report

*Prepared for:*

Andrea M. Dunn

National Energy Technology Laboratory  
U.S. Department of Energy  
626 Cochrans Mill Road  
PO Box 10940  
Pittsburgh, PA 15236-0940

DOE Cooperative Agreement No. DE-FC26-05NT42592

*Prepared by:*

Marc D. Kurz  
Loreal V. Heebink  
Steven A. Smith  
Erick J. Zacher

Energy & Environmental Research Center  
University of North Dakota  
15 North 23rd Street, Stop 9018  
Grand Forks, ND 58202-9018

## **EERC DISCLAIMER**

**LEGAL NOTICE** This research report was prepared by the Energy & Environmental Research Center (EERC), an agency of the University of North Dakota, as an account of work sponsored by the U.S. Department of Energy (DOE). Because of the research nature of the work performed, neither the EERC nor any of its employees makes any warranty, express or implied, or assumes any legal liability or responsibility for the accuracy, completeness, or usefulness of any information, apparatus, product, or process disclosed or represents that its use would not infringe privately owned rights. Reference herein to any specific commercial product, process, or service by trade name, trademark, manufacturer, or otherwise does not necessarily constitute or imply its endorsement or recommendation by the EERC.

## **ACKNOWLEDGMENT**

This material is based upon work supported by the DOE NETL under Award Number DE-FC26-05NT42592.

The Plains CO<sub>2</sub> Reduction (PCOR) Partnership team would like to thank Jonathan LaBonte, who is no longer employed at the EERC, for his efforts contributing to this report.

## **DOE DISCLAIMER**

This report was prepared as an account of work sponsored by an agency of the United States Government. Neither the United States Government, nor any agency thereof, nor any of their employees, makes any warranty, express or implied, or assumes any legal liability or responsibility for the accuracy, completeness, or usefulness of any information, apparatus, product, or process disclosed, or represents that its use would not infringe privately owned rights. Reference herein to any specific commercial product, process, or service by trade name, trademark, manufacturer, or otherwise does not necessarily constitute or imply its endorsement, recommendation, or favoring by the United States Government or any agency thereof. The views and opinions of authors expressed herein do not necessarily state or reflect those of the United States Government or any agency thereof.

## **NDIC DISCLAIMER**

This report was prepared by the EERC pursuant to an agreement partially funded by the Industrial Commission of North Dakota, and neither the EERC nor any of its subcontractors nor the North Dakota Industrial Commission nor any person acting on behalf of either:

- (A) Makes any warranty or representation, express or implied, with respect to the accuracy, completeness, or usefulness of the information contained in this report or that the use of any information, apparatus, method, or process disclosed in this report may not infringe privately owned rights; or

- (B) Assumes any liabilities with respect to the use of, or for damages resulting from the use of, any information, apparatus, method, or process disclosed in this report.

Reference herein to any specific commercial product, process, or service by trade name, trademark, manufacturer, or otherwise does not necessarily constitute or imply its endorsement, recommendation, or favoring by the North Dakota Industrial Commission. The views and opinions of authors expressed herein do not necessarily state or reflect those of the North Dakota Industrial Commission.

## TABLE OF CONTENTS

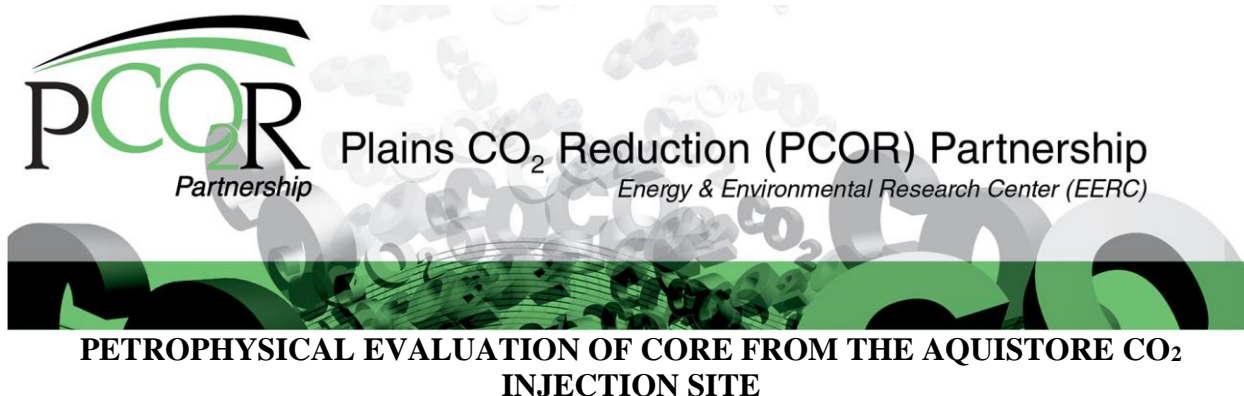
LIST OF FIGURES .....	ii
LIST OF TABLES .....	ii
EXECUTIVE SUMMARY .....	iii
INTRODUCTION .....	1
SAMPLE SELECTION AND METHODS OF ANALYSIS .....	2
Sample Selection .....	2
Methods of Analysis.....	3
Activity 1 (Tasks 1–3).....	3
Task 1 – Sample Preparation .....	3
Task 2 – Petrographic Analysis .....	3
Task 3 – Bulk Volume, Grain Density, and Porosity .....	6
Activity 2 (Tasks 4–6).....	6
Task 4 – SEM and XRD Analysis .....	6
Task 5 – Gas Permeability Determination .....	6
Task 6 – Liquid Permeability Determination .....	7
Activity 3 (Task 7) .....	7
Task 7 – CO <sub>2</sub> –Brine Relative Permeability Determination .....	7
SUMMARY OF KEY OBSERVATIONS .....	7
Characterization of Core Samples .....	7
Relative Permeability Evaluation .....	16
Recommendations for Future Work .....	17
ANALYTICAL TECHNIQUES.....	Appendix A
DATA SHEETS.....	Appendix B

## LIST OF FIGURES

1	Location map of PTRC_INJ_5-6-2-8 W2M well .....	1
2	Initial view of core .....	2
3	Core stratigraphic column with selected core locations .....	4
4	Example thin-section showing the distribution of quartz (white) and glauconite (green) in this sample .....	14
5	SEM image depicting glauconite weathering.....	15
6	SEM image representative of the formation of an iron-rich phase .....	16
7	Graph of relative permeability for simulated formation brine ( $K_{rw}$ ) and $CO_2$ ( $K_{rg}$ ) .....	17

## LIST OF TABLES

1	Sample Information and Indication of Analyses Performed per Activity .....	5
2	Summary of Petrographic and Petrophysical Properties Highlighting the Units .....	8
3	Petrographic and Petrophysical Properties Summary, Including Sample Photo and Thin-Section Image .....	9



## EXECUTIVE SUMMARY

The Energy and Environmental Research Center (EERC), through the Plains CO<sub>2</sub> Reduction (PCOR) Partnership and in collaboration with the Petroleum Technology Research Centre (PTRC), analyzed rock samples from a well near Estevan, Saskatchewan, as part of the ongoing efforts to characterize the subsurface for potential CO<sub>2</sub> injection and long-term storage. These samples were characterized to accomplish two key goals. The first goal was to provide the PTRC with insight into the lithology, porosity, and permeability of a proposed injection target for a small-scale demonstration project. The second goal was the utilization of the data by the EERC in the development of static geologic models to be used for dynamic simulation of CO<sub>2</sub> injection and storage scenarios. This report details the core analysis conducted and provides a summary of key petrographic and petrophysical properties attained.

In late August 2012, core was collected from a wellbore that penetrated the basal Deadwood Formation currently being evaluated for CO<sub>2</sub> storage as part of the PTRC Aquistore Project. The EERC was invited to view and provide geological descriptions of the 19.2 m (63 feet) of core collected from the lowermost section of the Deadwood Formation. Following the macroscopic description, twenty samples were collected spanning the 63-foot length and representative of the heterogeneities thought to exist through the injection target.

The EERC conducted several analyses on the well samples to determine mineralogy, porosity, and permeability. Specific tests included gas porosimetry and petrographic analysis via thin sections and gas porosimetry on all samples; scanning electron microscopy (SEM), x-ray diffraction (XRD), and permeability to gas and liquid on a select subset of samples; and CO<sub>2</sub>-brine relative permeability testing on one sample.

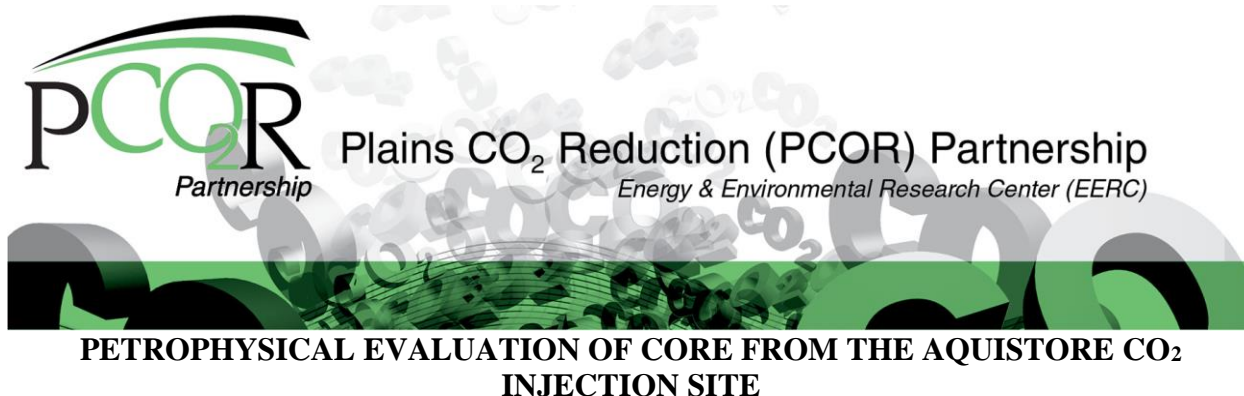
The samples evaluated from the lower Deadwood Formation are sandstones dominated by well-compacted quartz sand with glauconite clay in varying stages of dissolution. Sample porosities ranged from 2.7% to as high as 15.9% and permeability to air values ranged from 0.002 mD to 137 mD. Of the 20 samples tested, six had less than 9% porosity. In each of these cases, the corresponding permeability value was less than 2 mD, implying that where porosity exists, it is likely not well connected.

Results of the thin-section and SEM analyses showed that the interval sampled is predominantly quartz and glauconite-rich sandstone with dolomite cementing. Evidence of compaction and solution weathering was evidenced by highly sutured grain boundaries. Intraparticle porosity exists as a result of mineral crushing and mineral dissolution, including glauconite dissolution. Quartz overgrowths and mineral dissolution were observed as well as occasional clay and iron oxide pore linings. SEM analysis showed evidence of dissolution or weathering of glauconite in varying stages. In some cases, this dissolution led to the formation of clays and a residual iron-rich phase, and, in other cases, the iron released by the glauconite dissolution was incorporated into pore-filling dolomite.

Based on the general stages of glauconite dissolution, only three samples were selected for semiquantitative XRD analysis to identify/verify the major phases present in the samples. An additional sample was analyzed to support the modeling effort. All four samples consisted primarily of quartz. Other mineral phases identified included dolomite, glauconite, montmorillonite, K-feldspar, and chlorite.

The steady-state relative permeability testing conducted at the EERC used simulated formation brine (300,000 ppm) and pure CO<sub>2</sub>. The steady-state method entails running various mixtures of CO<sub>2</sub> and brine through the sample, from 100% brine and 0% CO<sub>2</sub> to 100% CO<sub>2</sub> and 0% brine. The permeability of the core to 100% brine was measured as 4.9 mD; however, CO<sub>2</sub> permeability was virtually nonexistent, except to 100% CO<sub>2</sub> with the presence of irreducible water saturation (44%). The permeability of CO<sub>2</sub> relative to the brine permeability is approximately 20% (or roughly 1 mD). Following the relative permeability testing, the plug was cleaned and dried and then retested for porosity. No changes in porosity were observed following relative permeability testing.

While the characterization work described herein was thorough with respect to the resources allocated, the Aquistore Project team may benefit by performing additional tests. Specifically, geochemical, mineralogical, and flow-through experimentation would provide additional insight into the injection and long-term distribution of CO<sub>2</sub> in this reservoir. Threshold intrusion pressures should be determined to understand and evaluate the quality of the sealing formation. Finally, mercury injection capillary entry pressure data will provide adequate estimates of pore throat size and distribution, ultimately providing a better understanding of the storage potential of this site.



## INTRODUCTION

In late August 2012, core was collected from the PTRC\_INJ\_5-6-2-8 W2M well located near Estevan in southern Saskatchewan, Canada (Figure 1). The well penetrates the basal Deadwood Formation currently being evaluated for carbon dioxide (CO<sub>2</sub>) storage as part of the Petroleum Technology Research Centre's (PTRC) Aquistore Project. The Energy & Environmental Research Center (EERC) was invited to view and provide geological descriptions of the 19.2-m (63 feet) core collected from the lowermost section of the Deadwood Formation. Following the macroscopic description, samples were collected and examined to determine the petrographic and petrophysical attributes of this interval of rock.

Select interpretations will be a primary input to local-scale geologic and simulation models of the proposed CO<sub>2</sub> injection site. The results of this investigation will be used to calibrate existing wireline logs to determine the degree of depth shifting necessary. The results will also be used to derive a series of log-based multimineral petrophysical interpretations of the well through the basal saline system.

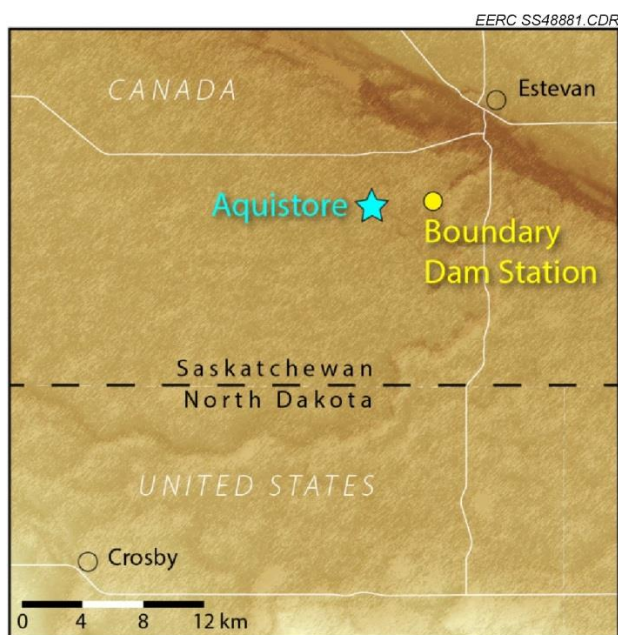


Figure 1. Location map of PTRC\_INJ\_5-6-2-8 W2M well.



The EERC conducted several tests on the samples from the well, analyzing for attributes, including mineralogy, porosity, and permeability. The project objectives were accomplished through the completion of three distinct activities consisting of several specific tasks. Each of the first two activities had a decision point regarding the specific work to be performed and samples to be tested in the subsequent activities. The tests included petrographic analysis via thin sections and gas pycnometer/porosimetry on all samples in Activity 1; scanning electron microscopy (SEM), x-ray diffraction (XRD), and permeability to gas and liquid on a select set of samples in Activity 2; and finally, CO<sub>2</sub>-brine relative permeability testing on one sample in Activity 3. This report presents a description of the sample selection, analysis methods, results, and discussion.

## **SAMPLE SELECTION AND METHODS OF ANALYSIS**

### **Sample Selection**

The core was housed in Calgary, Alberta, and was unwrapped for its initial viewing during the week of November 5, 2012. At the time of viewing, the core was not slabbed (whole core), as shown in Figure 2. During the initial viewing, the core was described and photographed by personnel from the EERC. Upon initial viewing, 11 informal units based on relatively small changes in lithologic character were observed. Specific attributes noted include grain size, grain sorting, mineral content, and observed sedimentary structures. These units also served as the basis for selecting sampling points for the laboratory work in order to provide information on zones of distinct lithologic character within each unit.

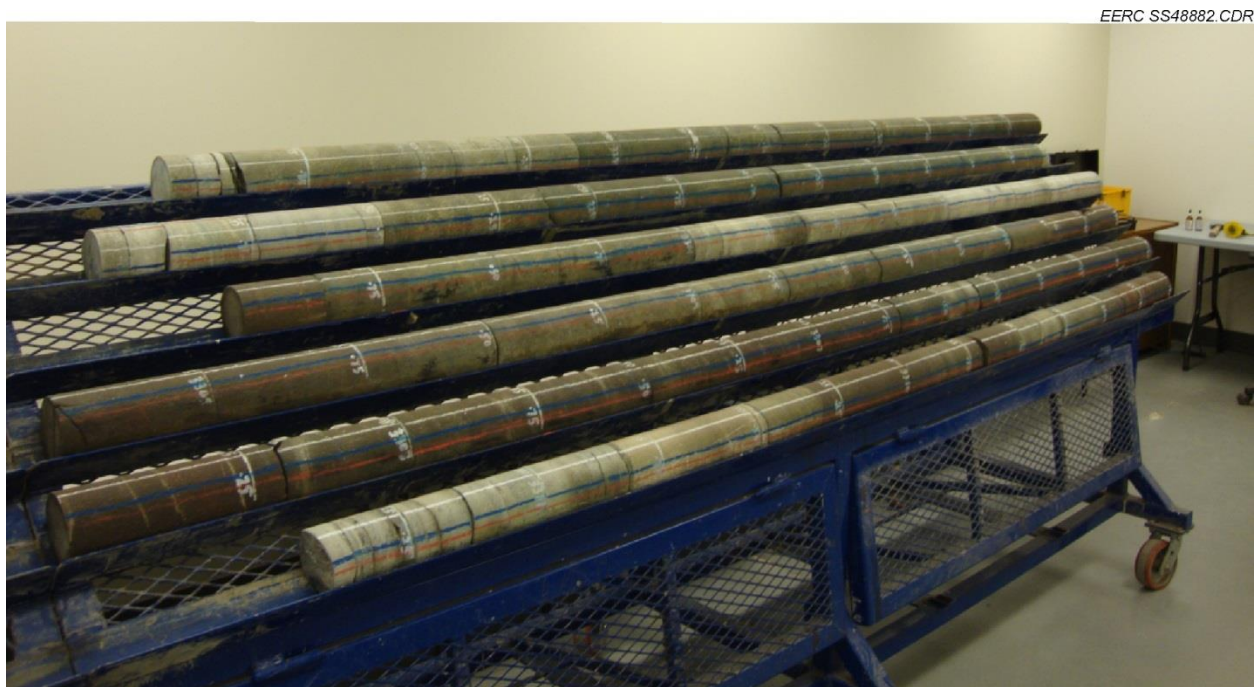


Figure 2. Initial view of core.

A total of 20 core plugs were selected and sampled from the examined core. Upon examination of the 20 plugs, it was determined that the original designation of 11 informal units would be scaled back to ten. This resulted as the mineralogy and grain-to-grain relationships were not observed. Figure 3 shows the location and orientation of sampled plugs. The samples were collected by representatives of TerraTek on behalf of the PTRC by Schlumberger Carbon Services at its Calgary, Alberta, facility the week of April 29, 2013. A representative of the EERC was present for the plug collection process. Samples were subsequently shipped to the EERC. The core plugs were cut to a diameter of 30 mm and a length of approximately 8 cm.

## **Methods of Analysis**

The samples collected were characterized in detail for petrographic and petrophysical attributes, including mineralogy, porosity, and permeability. The analyses were grouped into three activities to allow for sample down-selection after the results of an activity were reviewed. Table 1 contains sample information and a matrix indicating the analyses performed on each sample for each activity. Detailed descriptions of the analytical methods are provided in Appendix A. A brief description of each technique is provided under each activity.

### **Activity 1 (Tasks 1–3)**

This activity encompassed the process of collecting core samples and performing the first phase of characterization. The information obtained from this initial investigation was used in a down-selection process to identify 11 plugs that were subjected to further characterization and testing.

#### ***Task 1 – Sample Preparation***

All samples were photographed to document the as-received state of the core, cataloged, and described macroscopically. The 20 core plugs were cleaned by a Dean–Stark method utilizing solvents to remove residual brine and/or salt evaporates prior to any physical testing. The samples were dried in a humidity chamber at 60°C and 40% relative humidity until tested for porosity.

#### ***Task 2 – Petrographic Analysis***

Several petrographic techniques were utilized to evaluate the mineralogy of the rocks. A portion of the fragments generated from taking four vertical and 16 horizontal plugs were cut (retaining orientation) to 3.5×2×1-cm billets, which were sent to Wagner Petrographics for thin-section preparation. The EERC then used optical microscopy with plane-polarized and reflective light to analyze and describe the thin sections. Microscale mineralogical interpretations from the thin sections included rock fabric (grain size and shape distribution, cementation, and/or mineral overgrowth), description of microstructure, and mineral presence. Additional petrographic techniques including XRD and SEM were performed on a subset of core samples in subsequent activities.

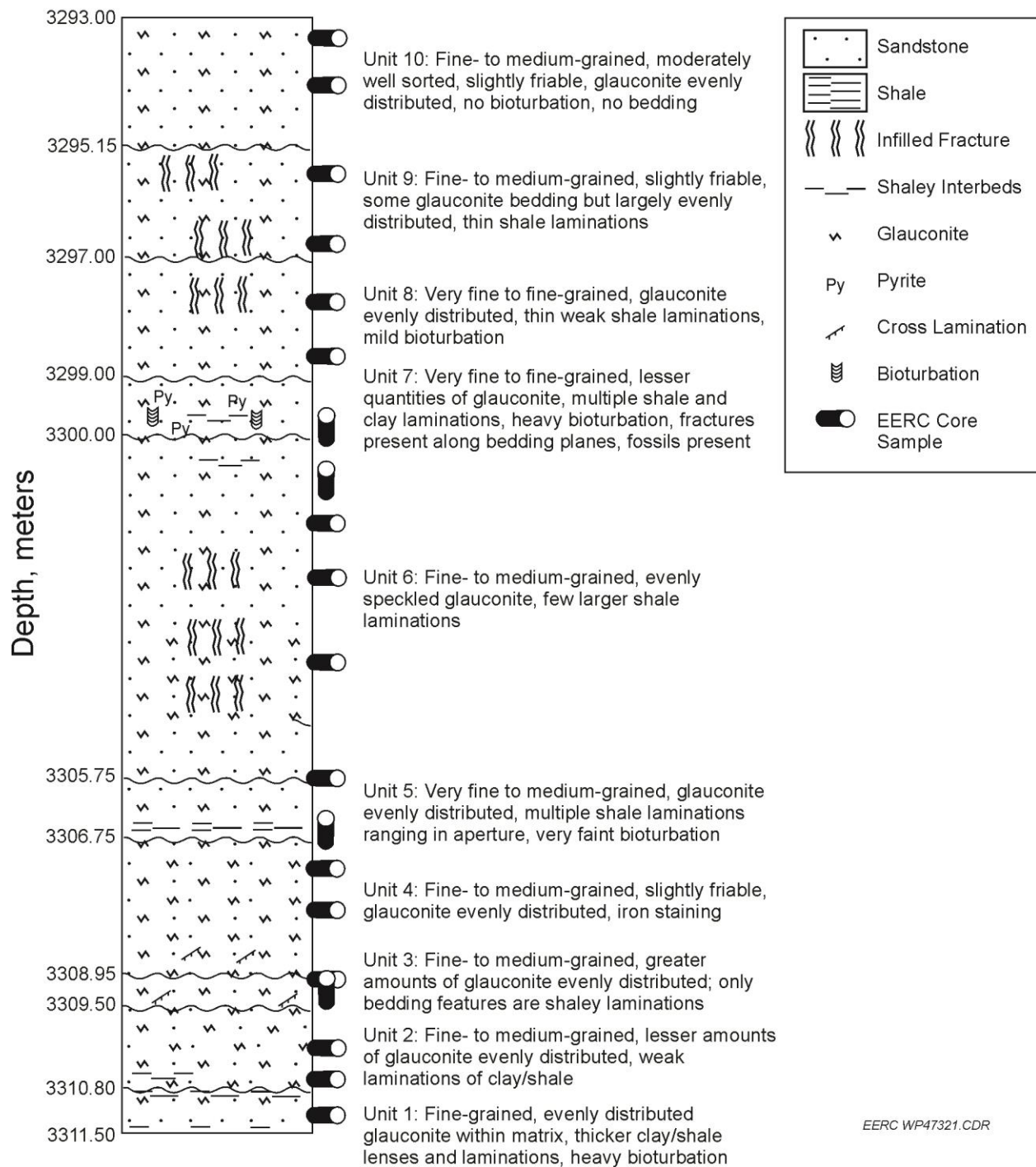


Figure 3. Core stratigraphic column with selected core locations.

**Table 1. Sample Information and Indication of Analyses Performed per Activity**

Sample	Depth, m	Plug Type	Unit	Activity 1	Activity 2				Activity 3
				Petrographic Analysis and Porosity	SEM	XRD	Gas Permeability	Liquid Permeability	Relative Permeability
1	3293.40	Horizontal	10	X <sup>1</sup>	X		X	X	
2	3294.12	Horizontal	10	X			X		
3	3295.60	Horizontal	9	X	X		X	X	
4	3296.75	Horizontal	9	X			X		
5	3297.76	Horizontal	8	X			X	X	
6	3298.58	Horizontal	8	X	X	X	X	X	
7	3299.80–3299.90	Vertical	7	X			X		
8	3300.63–3300.75	Vertical	6	X	X		X	X	
9	3301.35	Horizontal	6	X	X		X	X	
10	3302.30	Horizontal	6	X			X		
11	3303.68	Horizontal	6	X	X	X	X	X	
12	3305.60	Horizontal	6	X			X		
13	3306.41–3306.50	Vertical	5	X	X		X	X	
14	3307.10	Horizontal	4	X			X		
15	3307.80	Horizontal	4	X	X	X	X		
16	3308.93	Horizontal	4	X			X		
17	3309.00–3309.10	Vertical	3	X	X		X		
18	3310.10	Horizontal	2	X	X		X	X <sup>2</sup>	X
19	3310.60	Horizontal	2	X			X		
20	3311.17	Horizontal	1	X	X	X	X	X	

<sup>1</sup> An X indicates that the analyses included in that activity were performed.

<sup>2</sup> Performed as part of the relative permeability task.

### ***Task 3 – Bulk Volume, Grain Density, and Porosity***

The bulk volume and density, skeletal/grain volume and density, and porosity of each cleaned and humidity oven-dried core were determined utilizing a digital caliper and a commercial-grade helium porosimeter. The technique utilizes Boyle's law equations to determine the grain volume, which is then subtracted from the bulk volume to yield the pore volume of the sample. These results were utilized further in permeability and relative permeability test calculations. Measurements were also used as direct inputs into static geologic models developed for the project.

### **Activity 2 (Tasks 4–6)**

Based on information obtained from sample testing performed in Activity 1, a subset of 11 core plugs was selected for additional analyses including petrographic analyses by SEM and XRD, gas permeability, and liquid permeability. These 11 samples include at least one sample from nine of the ten unit designations and cover the range of porosity values and a range of glauconite content as indicated by thin-section analyses. The information obtained during this task was evaluated and used to identify a subset of three cores for potential use in Activity 3.

### ***Task 4 – SEM and XRD Analysis***

Thin sections were utilized for analysis by SEM, and core pieces from the remaining thin-section billet were ground for analysis by XRD. These analyses were used in conjunction with the results of thin-section analysis to provide additional information on characteristics such as the bulk mineralogy and textural, elemental, and mineralogical composition of the samples. Specific information obtained includes the identification of the major mineral phases and clay types present (i.e., illite, muscovite, smectite, glauconite, etc.). Because of the relatively “clean” nature of these samples, detailed clay speciation was not performed. The results from the techniques were interpreted as a package to provide a concise characterization of the rocks. X-ray fluorescence (XRF) was proposed with SEM and XRD; however, it was determined that, given the characterization through thin-section analyses, XRF would not be necessary as an interpretation aid.

- **SEM techniques** – SEM techniques were used to evaluate the textural, elemental, and mineralogical composition of the samples using backscattered electron imaging and energy-dispersive spectrometry (EDS). EDS was used to create maps showing the mineralogical composition of the samples.
- **XRD analysis** – XRD is the standard method for determining bulk mineralogy of materials. The complementary use of SEM data enhances bulk mineral identification. Rietveld refinement was used to quantify the mineralogical composition of the samples.

### ***Task 5 – Gas Permeability Determination***

Gas permeability was determined for each sample utilizing a steady-state standard method (ASTM D4525). While much of the work in Activity 2 focused on a subset of 11 plug samples, it was decided that all 20 plugs would be tested for permeability. This decision would provide a

porosity/permeability relationship for each sample as well as aid in the selection of samples for relative permeability. This method determines the specific permeability of nitrogen through the core material and a Klinkenberg correction coefficient is determined to correct for gas slippage. The gas permeability was determined under low confining stress (800 psi).

### ***Task 6 – Liquid Permeability Determination***

A permeameter was utilized to determine liquid permeability of each core using a deaerated water–brine solution. An 800-psi confining pressure was applied as the solution flowed and was measured through the sample. The test was run at steady state and at multiple pressure conditions to ensure accuracy of the measurements. Samples used in this test were determined to have potential for relative permeability testing.

### **Activity 3 (Task 7)**

Based on information obtained from project tasks in both Activities 1 and 2, a subset of three cores was selected for relative permeability testing. At the time of this reporting, only one of the samples has been completed, and data pertaining to this sample are provided.

### ***Task 7 – CO<sub>2</sub>–Brine Relative Permeability Determination***

Relative permeability testing was conducted on one of the selected core samples and included the determination of a drainage curve utilizing CO<sub>2</sub> and brine. The testing utilized the steady-state method where predetermined ratios of CO<sub>2</sub> and brine are set at a known flow rate and pumped through the core plug until a constant pressure drop is achieved. The brine utilized was a synthetic mixture of salts similar to the chemistry of the actual formation brine, and prepared according to data provided by PTRC to match existing relative permeability tests. Data from the steady-state testing was then used to construct relative permeability drainage curves for use in the related geophysical modeling efforts.

## **SUMMARY OF KEY OBSERVATIONS**

### **Characterization of Core Samples**

The core was described macroscopically at the initial viewing to identify lithologic and mineralogic changes for core to log correlation and sample point identification. Following the sampling process and receipt of core plugs, the specific samples were described macroscopically since different aspects of the core could be visualized. Based on the macroscopic view of the samples, the initial unit divisions and points of unit separation were adjusted into ten new informal units, as shown in Figure 3.

Table 2 provides a summary of the petrographic and petrophysical properties determined. Included are the sample locations; laboratory-derived grain density, porosity, and gas and liquid permeability data; and dominant mineral phases determined by SEM and XRD. Data from all characterization activities are provided as a series of data sheets in Appendix B. Sample photos and photomicrographs obtained from thin-section analyses were added in Table 3 to provide a

**Table 2. Summary of Petrographic and Petrophysical Properties Highlighting the Units**

Sample	Depth, m	Unit	Grain Density, g/cm <sup>3</sup>	Porosity, vol%	Gas Permeability, <sup>1</sup> mD	Liquid Permeability, mD	SEM Dominant Mineral Phases <sup>2</sup>	XRD Dominant Mineral Phases <sup>2</sup>
1	3293.40	10	2.7	14.5	121.43	92.2	Q, G	NT <sup>3</sup>
2	3294.12	10	2.7	12.8	21.19	NDS <sup>4</sup>	NDS	NDS
3	3295.60	9	2.7	11.6	79.97	53.9	Q, G	NT
4	3296.75	9	2.7	10.2	23.20	NDS	NDS	NDS
5	3297.76	8	2.7	6.1	1.62	NDS	NDS	NDS
6	3298.58	8	2.7	6.2	0.04	0.026	Q, G	Q, G
7	3299.80–3299.90 <sup>5</sup>	7	2.7	3.5	0.002–0.006	NDS	NDS	NDS
8	3300.63–3300.75 <sup>5</sup>	6	2.7	11.9	58.07	29.9	Q, D, G	NT
9	3301.35	6	2.7	9.9	44.93	13.2	Q, D	NT
10	3302.30	6	2.7	15.9	136.53	NDS	NDS	NDS
11	3303.68	6	2.7	13.9	312.3	254.3	Q, G	Q, D, M, G
12	3305.60	6	2.7	10.4	35.37	NDS	NDS	NDS
13	3306.41–3306.50 <sup>5</sup>	5	2.7	8.6	0.02	0.014	Q, G, K-F	NT
14	3307.10	4	2.7	14.5	57.34	NDS	NDS	NDS
15	3307.80	4	2.8	11.1	3.96	NDS	Q, H, G, D	Q, D, G
16	3308.93	4	2.7	11.7	16.65	NDS	NDS	NDS
17	3309.00–3309.10 <sup>5</sup>	3	2.7	11.5	0.29	NDS	Q, G	NT
18	3310.10	2	2.7	11.3	13.25	4.9 <sup>6</sup>	Q, D, G	NT
19	3310.60	2	2.7	8.1	0.03	NDS	NDS	NDS
20	3311.17	1	2.7	2.7	0.04	0.026	Q, I, G, K-F	Q, K-F, C, G

<sup>1</sup> Klinkenberg corrected values with nitrogen gas and 800-psi confining pressure.

<sup>2</sup> Quartz (Q), Apatite (A), Dolomite (D), Glauconite (G), Potassium Feldspar (K-F), Montmorillonite (M), Hematite (H), Illite (I), and Chlorite (C). These are listed in order of prevalence based on SEM mineral map relative weight percentage with only mineral phases greater than 10% considered to be dominant mineral phases. These are listed in order of XRD semiquantitative crystalline relative weight percentage. The amorphous glauconite content cannot be taken into account with XRD. A complete listing of minerals associated with each sample is found in Appendix B.

<sup>3</sup> NT = Not tested because of sample homogeneity based on thin-section analysis.

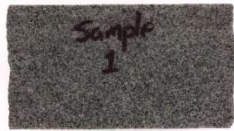
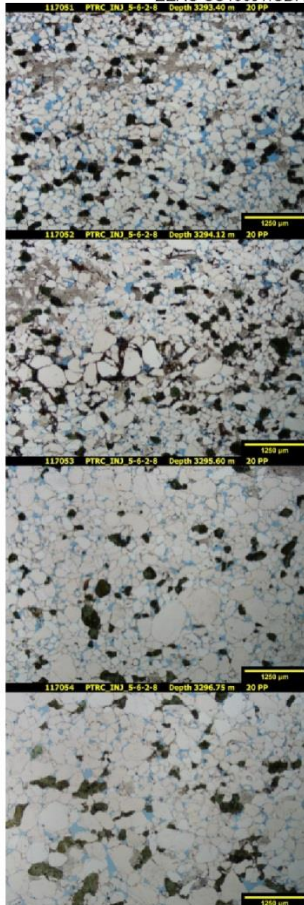


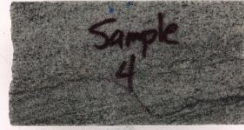
<sup>4</sup> NDS = Not down-selected for Activity 2.

<sup>5</sup> Depth intervals are vertical plugs.

<sup>6</sup> The value was obtained during relative permeability testing, which also utilized a higher brine concentration.



**Table 3. Petrographic and Petrophysical Properties Summary, Including Sample Photo and Thin-Section Image**

Sample	Depth, m	Unit	Porosity, vol%	Permeability, mD		Dominant Mineral Phases <sup>2</sup>		Sample Photo (scale = 2 cm)	Thin Section, 20×PP EERC SS48891 CDR
				Gas <sup>1</sup>	Liquid	SEM	XRD		
1	3293.40	10	14.5	121.43	92.2	Q, G	NT <sup>3</sup>		
								2.5 cm	
2	3294.12	10	12.8	21.19	NDS <sup>4</sup>	NDS	NDS		
								2.5 cm	
3	3295.60	9	11.6	79.97	53.9	Q, G	NT		
								2.5 cm	
4	3296.75	9	10.2	23.20	NDS	NDS	NDS		
								2.5 cm	

<sup>1</sup> Klinkenberg corrected values with nitrogen gas and 800-psi confining pressure.

<sup>2</sup> Quartz (Q), Apatite (A), Dolomite (D), Glauconite (G), Potassium Feldspar (K-F), Montmorillonite (M), Hematite (H), Illite (I), and Chlorite (C). These are listed in order of prevalence based on SEM mineral map relative weight percentage with only mineral phases greater than 10% considered to be dominant mineral phases. These are listed in order of XRD semiquantitative crystalline relative weight percentage. The amorphous glauconite content cannot be taken into account with XRD. A complete listing of minerals associated with each sample is found in Appendix B.

<sup>3</sup> NT = Not tested because of sample homogeneity based on thin-section analysis.

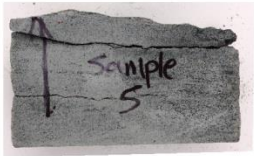

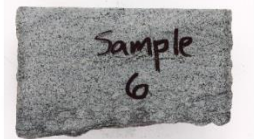
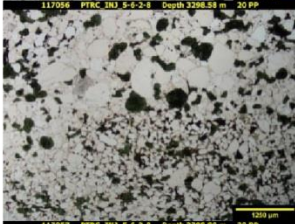
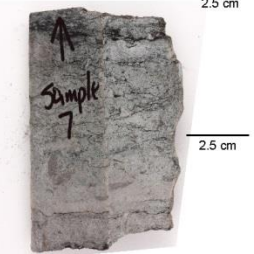


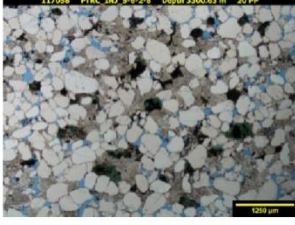
<sup>4</sup> NDS = Not down-selected for Activity 2.

<sup>5</sup> The value was obtained during relative permeability testing, which also utilized a higher brine concentration.

Continued...



**Table 3. Petrographic and Petrophysical Properties Summary, Including Sample Photo and Thin-Section Image (continued)**

Sample	Depth, m	Unit	Porosity, vol%	Permeability, mD		Dominant Mineral Phases <sup>2</sup>		Sample Photo (scale = 2 cm)	Thin Section, 20×PP EERC SS48890 CDR
				Gas <sup>1</sup>	Liquid	SEM	XRD		
5	3297.76	8	1.62		NDS	NDS	NDS		
6	3298.58	8	6.2	0.04	0.026	Q, G	Q, G		
7	3299.80– 3299.90	7	3.5	0.002– 0.006	NDS	NDS	NDS		
8	3300.63– 3300.75	6	11.9	58.07	29.9	Q, D, G	NT		

<sup>1</sup> Klinkenberg corrected values with nitrogen gas and 800-psi confining pressure.

<sup>2</sup> Quartz (Q), Apatite (A), Dolomite (D), Glauconite (G), Potassium Feldspar (K-F), Montmorillonite (M), Hematite (H), Illite (I), and Chlorite (C). These are listed in order of prevalence based on SEM mineral map relative weight percentage with only mineral phases greater than 10% considered to be dominant mineral phases. These are listed in order of XRD semiquantitative crystalline relative weight percentage. The amorphous glauconite content cannot be taken into account with XRD. A complete listing of minerals associated with each sample is found in Appendix B.


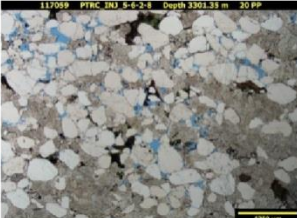
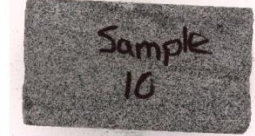
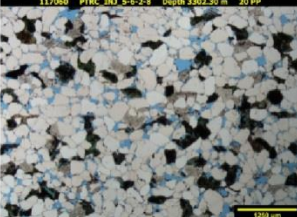

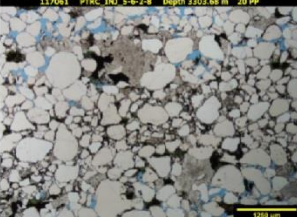
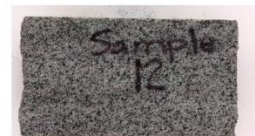
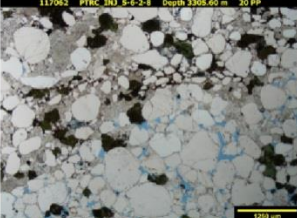
<sup>3</sup> NT = Not tested because of sample homogeneity based on thin-section analysis.

<sup>4</sup> NDS = Not down-selected for Activity 2.

<sup>5</sup> The value was obtained during relative permeability testing, which also utilized a higher brine concentration.

Continued...

**Table 3. Petrographic and Petrophysical Properties Summary, Including Sample Photo and Thin-Section Image (continued)**

Sample	Depth, m	Unit	Porosity, vol%	Permeability, mD		Dominant Mineral Phases <sup>2</sup>		Sample Photo (scale = 2 cm)	Thin Section, 20×PP <small>EERC SS48889.CDR</small>
				Gas <sup>1</sup>	Liquid	SEM	XRD		
9	3301.35	6	9.9	44.93	13.2	Q, D	NT		
10	3302.30	6	15.9	136.53	NDS	NDS	NDS		
11	3303.68	6	13.9	312.3	254.3	Q, G	Q, D, M, G		
12	3305.60	6	10.4	35.37	NDS	NDS	NDS		

<sup>1</sup> Klinkenberg corrected values with nitrogen gas and 800-psi confining pressure.

<sup>2</sup> Quartz (Q), Apatite (A), Dolomite (D), Glauconite (G), Potassium Feldspar (K-F), Montmorillonite (M), Hematite (H), Illite (I), and Chlorite (C). These are listed in order of prevalence based on SEM mineral map relative weight percentage with only mineral phases greater than 10% considered to be dominant mineral phases. These are listed in order of XRD semiquantitative crystalline relative weight percentage. The amorphous glauconite content cannot be taken into account with XRD. A complete listing of minerals associated with each sample is found in Appendix B.


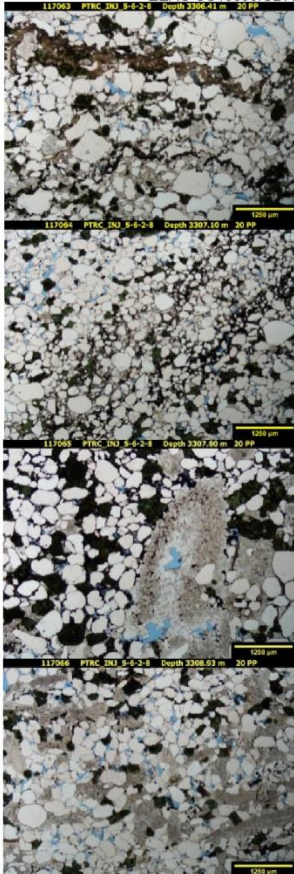
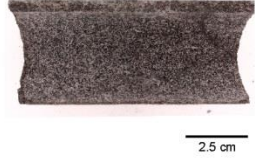


<sup>3</sup> NT = Not tested because of sample homogeneity based on thin-section analysis.

<sup>4</sup> NDS = Not down-selected for Activity 2.

<sup>5</sup> The value was obtained during relative permeability testing, which also utilized a higher brine concentration.

Continued...

**Table 3. Petrographic and Petrophysical Properties Summary, Including Sample Photo and Thin-Section Image (continued)**

Sample	Depth, m	Unit	Porosity, vol%	Permeability, mD		Dominant Mineral Phases <sup>2</sup>		Sample Photo (scale = 2 cm)	Thin Section, 20×PP
				Gas <sup>1</sup>	Liquid	SEM	XRD		
13	3306.41–3306.50	5	8.6	0.02	0.014	Q, G, K-F	NT		
14	3307.10	4	14.5	57.34	NDS	NDS	NDS		
15	3307.80	4	11.1	3.96	NDS	Q, H, G, D	Q, D, G		
16	3308.93	4	11.7	16.65	NDS	NDS	NDS		

<sup>1</sup> Klinkenberg corrected values with nitrogen gas and 800-psi confining pressure.

<sup>2</sup> Quartz (Q), Apatite (A), Dolomite (D), Glauconite (G), Potassium Feldspar (K-F), Montmorillonite (M), Hematite (H), Illite (I), and Chlorite (C). These are listed in order of prevalence based on SEM mineral map relative weight percentage with only mineral phases greater than 10% considered to be dominant mineral phases. These are listed in order of XRD semiquantitative crystalline relative weight percentage. The amorphous glauconite content cannot be taken into account with XRD. A complete listing of minerals associated with each sample is found in Appendix B.

<sup>3</sup> NT = Not tested because of sample homogeneity based on thin-section analysis.


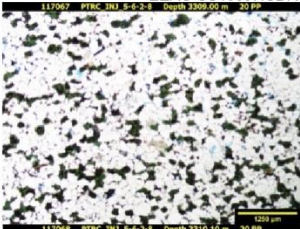






<sup>4</sup> NDS = Not down-selected for Activity 2.

<sup>5</sup> The value was obtained during relative permeability testing, which also utilized a higher brine concentration.

Continued...



**Table 3. Petrographic and Petrophysical Properties Summary, Including Sample Photo and Thin-Section Image (continued)**

Sample	Depth, m	Unit	Porosity, vol%	Permeability, mD		Dominant Mineral Phases <sup>2</sup>		Sample Photo (scale = 2 cm)	Thin Section, 20×PP EERC SS48887.CDR
				Gas <sup>1</sup>	Liquid	SEM	XRD		
17	3309.00– 3309.10	3	11.5	0.29	NDS	Q, G	NT		
18	3310.10	2	11.3	13.25	4.9 <sup>5</sup>	Q, D, G	NT		
19	3310.60	2	8.1	0.03	NDS	NDS	NDS		
20	3311.17	1	2.7	0.04	0.026	Q, I, G, K-F	Q, K-F, C, G		

<sup>1</sup> Klinkenberg corrected values with nitrogen gas and 800-psi confining pressure.<sup>2</sup> Quartz (Q), Apatite (A), Dolomite (D), Glauconite (G), Potassium Feldspar (K-F), Montmorillonite (M), Hematite (H), Illite (I), and Chlorite (C). These are listed in order of prevalence based on SEM mineral map relative weight percentage with only mineral phases greater than 10% considered to be dominant mineral phases. These are listed in order of XRD semiquantitative crystalline relative weight percentage. The amorphous glauconite content cannot be taken into account with XRD. A complete listing of minerals associated with each sample is found in Appendix B.<sup>3</sup> NT = Not tested because of sample homogeneity based on thin-section analysis.<sup>4</sup> NDS = Not down-selected for Activity 2.<sup>5</sup> The value was obtained during relative permeability testing, which also utilized a higher brine concentration.

visual view of the sampling points through the core to correspond to the data, excluding the grain density.

The sandstones evaluated from the lower Deadwood Formation are dominated by well-compacted quartz sand with glauconite clay in varying stages of dissolution. Samples range in porosity from 2.7% to as high as 15.9% with gas permeability values ranging from 0.002 mD to 136.53 mD. Of the 20 samples tested, six exhibited porosity of less than 9%. In each of these cases, the corresponding permeability value was less than 2 mD, implying that where porosity exists in these samples, it is likely not well connected.

The thin-section analyses showed that much of the core is predominantly quartz and glauconite-rich sandstone with dolomite cement. Glauconite is a bright green, iron- and potassium-rich mineral that forms from the weathering of iron-bearing micas (such as biotite) under reducing conditions found in some shallow marine environments. Evidence of compaction and solution weathering was depicted by the highly sutured grain boundaries. Intraparticle porosity was created through mineral crushing and dissolution. Quartz overgrowths and mineral dissolution were observed. Clay and iron oxide pore linings were occasionally observed. An example thin-section photomicrograph from Sample 18 is shown in Figure 4.

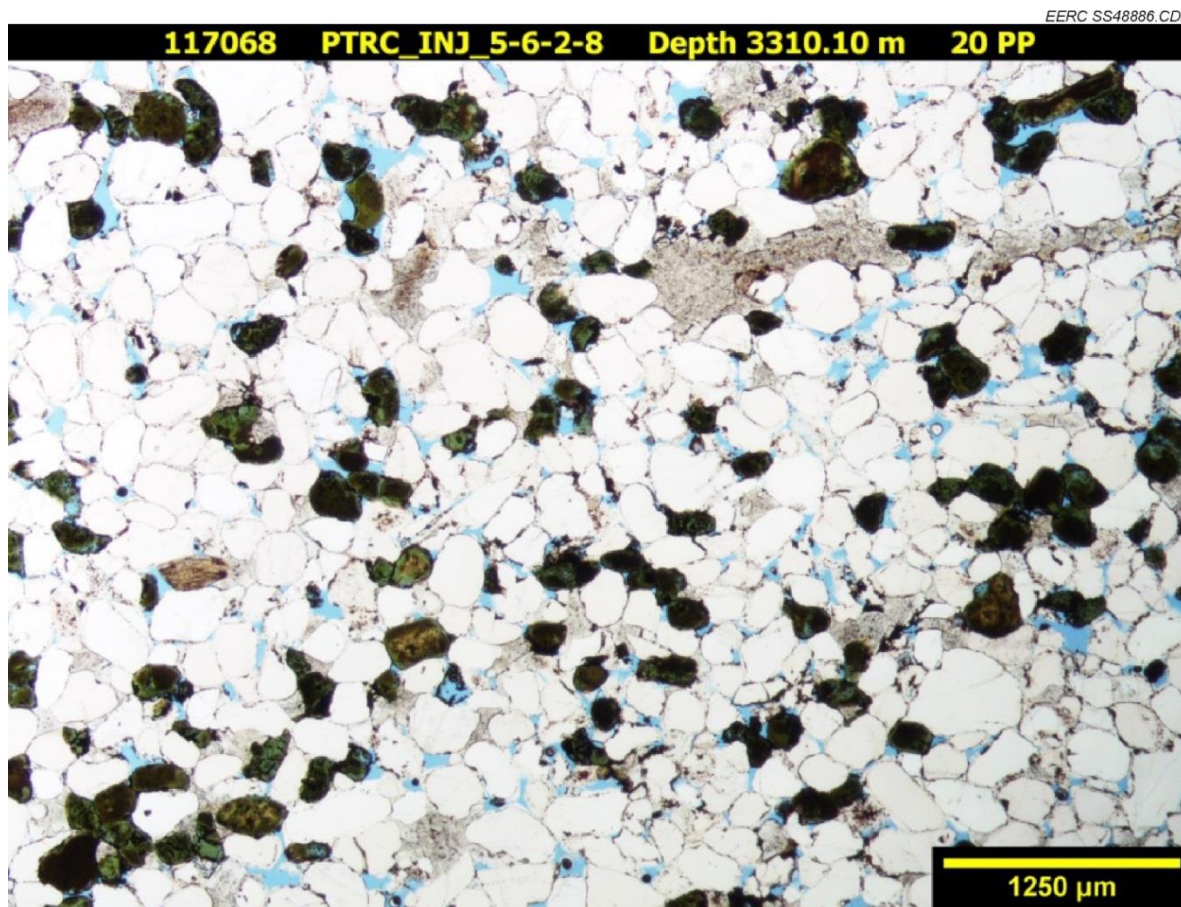


Figure 4. Example thin-section showing the distribution of quartz (white) and glauconite (green) in this sample.



SEM morphologies from the analyses of the thin sections of the samples in Activity 2 showed the abundance of quartz in these sandstone samples and indicated the occurrence of chemical compaction (mostly dissolution). Dissolution or weathering of glauconite was evident and appeared to be present in varying stages based on visual inspection of the SEM images. An example is provided in Figure 5. In some cases, this dissolution has led to the formation of clays and an iron-rich phase being left behind, often edging where the glauconite was or still is partially, as shown in Figure 6. In other areas, the iron released by the dissolution of glauconite is incorporated into pore-filling dolomite. Based on the images obtained, a portion of the porosity may be from the dissolution of glauconite.

Based on the general stages of glauconite dissolution, only three samples were selected for semiquantitative XRD analysis to identify/verify the major phases present in the samples. An additional sample was analyzed to support the modeling effort. Not all down-selected Activity 2 samples were analyzed by XRD because glauconite, which is a major mineral phase in many of the samples, is generally amorphous, making it difficult to provide quantitative XRD results. All four samples consisted primarily of quartz. Other phases identified as crystalline mineral phases included dolomite, glauconite, montmorillonite, K-feldspar, and chlorite. The crystalline mineral phases identified in the four samples are noted on a per-sample basis in Appendix B.

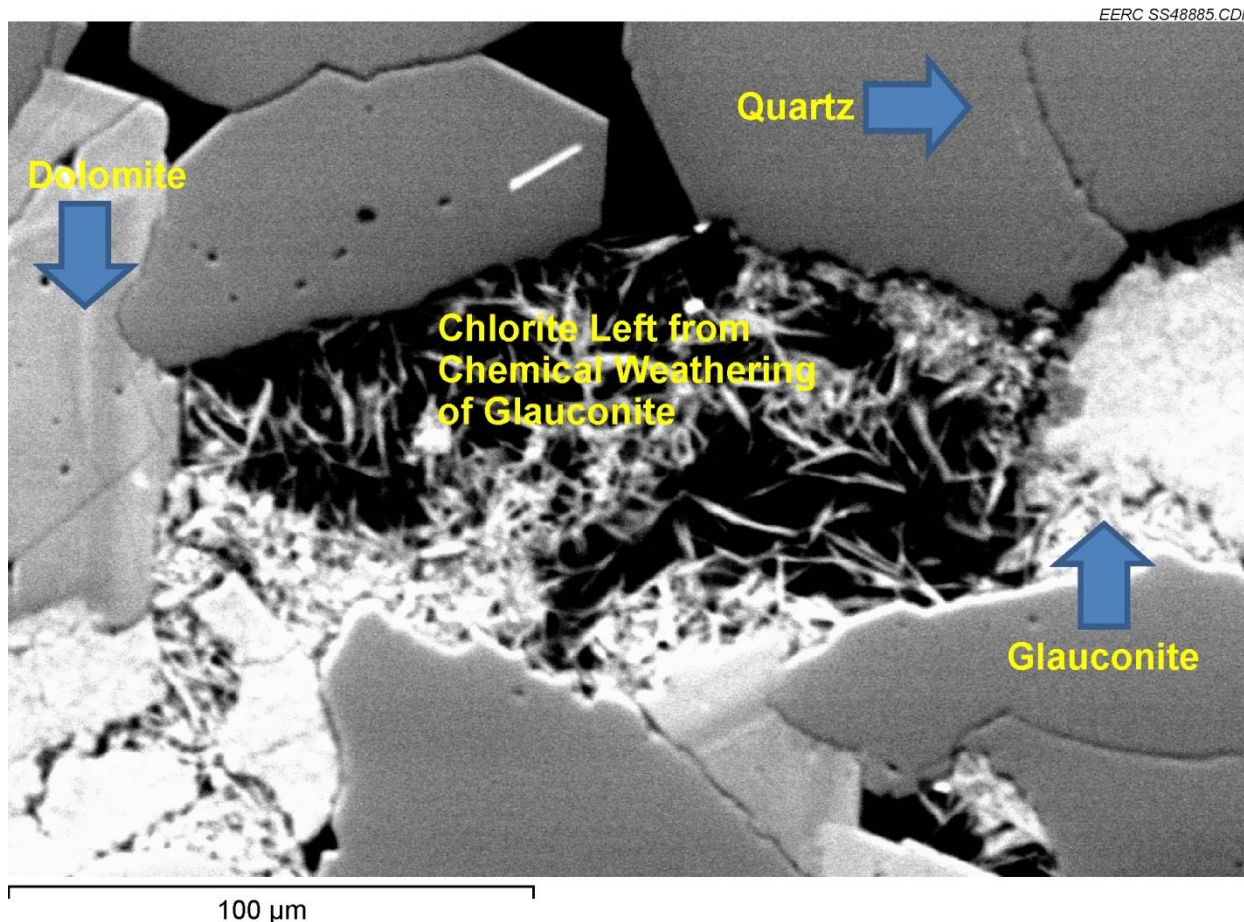


Figure 5. SEM image depicting glauconite weathering.

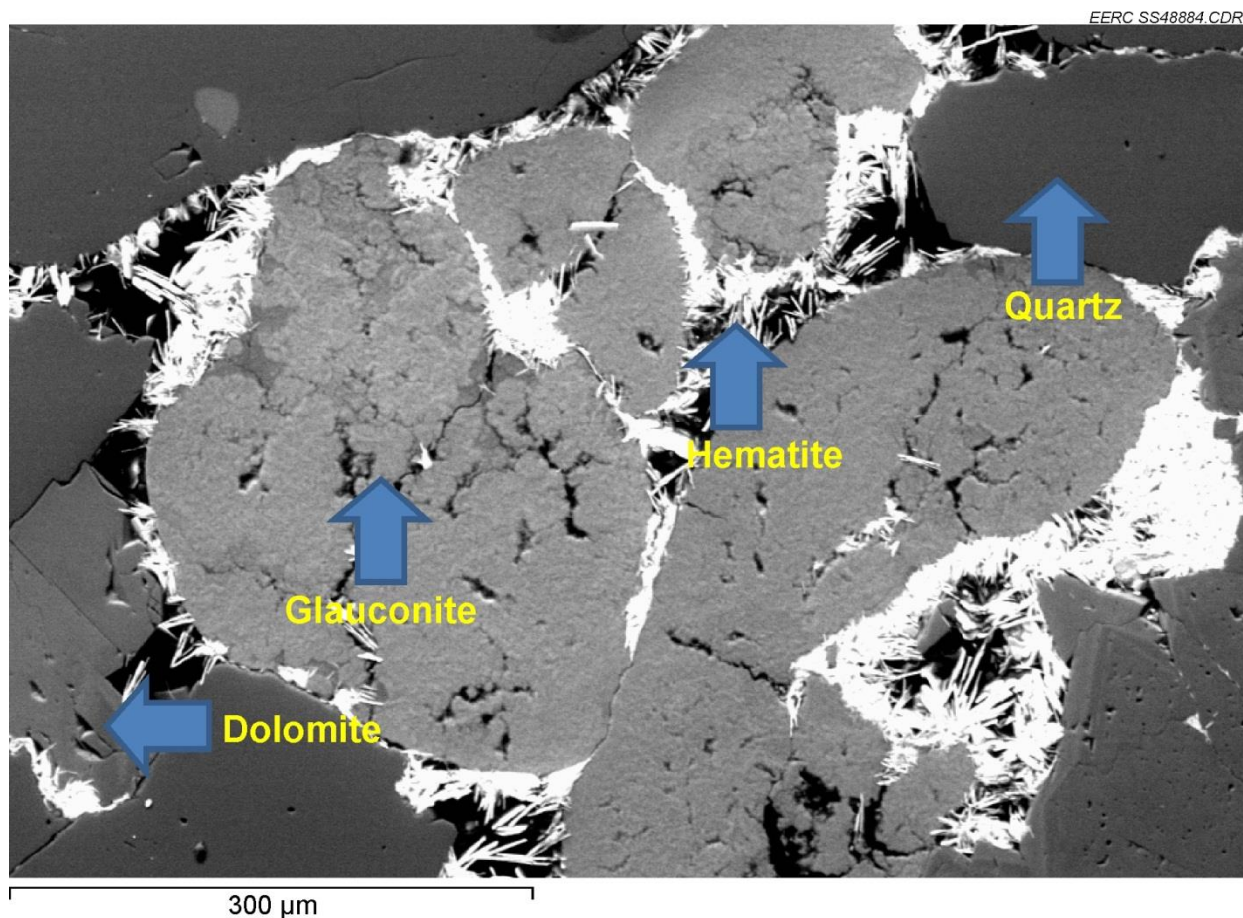


Figure 6. SEM image representative of the formation of an iron-rich phase.

### Relative Permeability Evaluation

Relative permeability is a specialized core test that calculates the relative rate at which supercritical CO<sub>2</sub> flows through water-saturated rock and also identifies irreducible water saturation (Swirr) at reservoir conditions. The steady-state relative permeability testing conducted at the EERC, utilizing a simulated formation brine and CO<sub>2</sub>, found that permeability to CO<sub>2</sub> is extremely low in the presence of brine, as shown in Figure 7. The permeability of the core to 100% brine was found to be 4.9 mD; however, the permeability is virtually nonexistent for CO<sub>2</sub> except for the case of 100% CO<sub>2</sub> with the presence of irreducible water saturation, which was determined to be 44%. The maximum permeability of CO<sub>2</sub> relative to the brine permeability is approximately 20% (or roughly 1 mD).

Following the relative permeability testing, the plug was cleaned of salts from the brine using methanol as a solvent in a Soxhlet extraction apparatus. It was then dried in the humidity oven and tested for porosity again. There were no porosity changes observed, so no additional evaluations using SEM or XRD were performed.

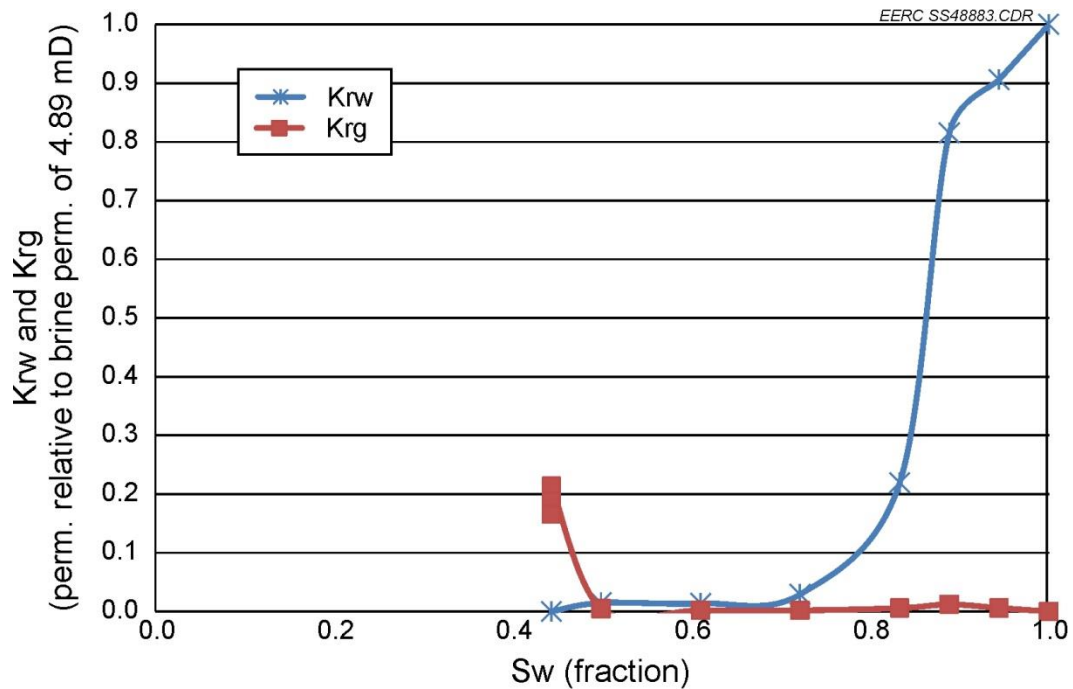


Figure 7. Graph of relative permeability for simulated formation brine (Krw) and CO<sub>2</sub> (Krg).

### Recommendations for Future Work

- Additional geochemical evaluations to determine the stability of glauconite and impacts it may have on injectivity at this site.
- Additional relative permeability work to better understand the CO<sub>2</sub> storage potential of this reservoir.
- Collection of additional core to determine the homogeneity of this reservoir laterally adjacent to the injection zone. Further mineralogical and flow-through testing to determine similarities and differences.



# **APPENDIX A**

## **ANALYTICAL TECHNIQUES**

## **ANALYTICAL TECHNIQUES**

### **THIN-SECTION PRODUCTION AND RELATED ANALYSES**

Thin sections were prepared by Wagner Petrographic. Billets were assigned an identification number, then trimmed to fit a microscope slide. The samples were dried at 150°F and cast in Columbia Blue-dyed epoxy. Billets were flattened/polished on a 125- $\mu$ m lap wheel and taken progressively to a 10- $\mu$ m lap wheel for polishing prior to adhesion to a glass microscope slide. After the curing process, excess material was cut off. Cutoff slides were thinned and polished to 30  $\mu$ m on a 6- $\mu$ m lap wheel. At this point, alizarin red and potassium ferricyanide stains were applied to aid in the identification of calcite and ferrous minerals.

The thin sections were analyzed and photographed using a petrographic microscope. Mineralogical assemblages and prevalence were determined and estimated through the use of standard optical techniques utilizing a combination of plane-polarized, cross-polarized, and reflective light. Photomicrographs were produced at 20 $\times$ , 50 $\times$ , 100 $\times$ , 200 $\times$ , and 500 $\times$  magnification (using 2 $\times$ , 5 $\times$ , 10 $\times$ , 20 $\times$ , and 50 $\times$  objectives) with plane-polarized light and with reflective light. Additional photographs depicting specific features were also collected.

#### **Effective Porosity**

Samples were cleaned through a Soxhlet/Dean–Stark extraction process. Core plugs were cleaned utilizing a 50/50 blend by volume of toluene and methanol. Dean–Stark was performed as a cleaning technique only and no calculations of residual fluids were performed. Toluene was used as the agent to extract water and oil, and methanol was utilized for the coextraction of residual brine and/or salt evaporates. The samples were distilled until no salts within the extraction system were detected with a silver nitrate solution. Each sample was allowed to air-dry in the fume hood to drive off solvent fumes prior to being placed in a humidifying chamber. The samples were dried in the chamber at 60°C and 40% relative humidity until the weight of the sample stabilized. All 20 samples were analyzed for effective porosity after stable weights were obtained from the humidity chamber.

Prior to porosity testing, bulk volume was determined utilizing a Vernier caliper. Five measurements for length and ten measurements for diameter were averaged for calculation of bulk volume. Dry sample mass was measured and divided by bulk volume to calculate bulk density.

Effective porosity testing was performed using the MetaRock PDP-300 research-grade helium pycnometer–porosimeter system, which exposes a known volume and pressure of helium gas to a chamber containing the dry sample. The test employs Boyle’s law technique and produces measurement of grain volume, which enables the calculation of porosity when compared with bulk volume.

After determining porosity of the humidified samples, several measurements on five core plugs dried completely in a convection oven at 116°C (241°F) were made to draw comparisons

between humidity-dried samples and convection-dried samples. The drying technique is a key consideration when evaluating porosity because excessive drying will dehydrate clays and yield erroneously high helium porosity values. Humidity drying will allow the rehydration of clay-bound waters of hydration. If significant clay minerals are present, an increase in helium porosity will be seen when the sample is dried completely (i.e., convection drying). According to Bush and Jenkins (1970), humidified drying will retain at least one to two layers of adsorbed water on the clay minerals' surfaces. Excessive drying can remove all water absorbed by the sample inducing errors to the calculated porosity and permeability. If no significant change in effective porosity is evident between humidified and convection-dried samples, it can be inferred that the clay content of the sample is low and either value can be reported as the true effective porosity. As shown in Table A-1, the porosity following humidified drying and convection drying was similar for four of the five samples. The increase in porosity noted in Sample 6 may indicate excessive drying of water in the sample.

### Gas Permeability

Permeability to gas measurements were performed in a gas (nitrogen [N<sub>2</sub>]) system at pressures up to 100 psi. The system is capable of measuring permeability at steady state from about 0.01 mD up to 1 Darcy, and is also capable of unsteady-state measurements for even lower permeability samples. A core sample of approximately 30 mm diameter and lengths up to approximately 10 cm is loaded into a Hassler-type core holder and a confining pressure of 800 psi is applied radially around the core. In this setup, the axial stress is not specified and varies with applied differential pressure. The system uses a mass flow controller or pressure regulator to apply a steady-state flow. High-accuracy differential transducers and flowmeters are used to determine the permeability at a variety of back pressures. Multiple conditions are tested for each sample, and the permeability is then corrected for gas slippage by finding the Klinkenberg corrected gas permeability from the data set. The Aquistore samples were tested after being stored in a humidified state (60°C, 40% relative humidity) but were permeability tested with dry nitrogen as the flowing gas.

### Permeability to Water

A permeameter or a set of liquid pumps is used to measure water permeability of a sample depending upon test conditions and sample type. A sample is loaded into a Hassler-type core holder and a confining pressure of 800 psi is applied radially around the sample. A deaerated

**Table A-1. Comparison of Effective Porosity Following Humidified Drying and Convection Drying**

Sample	Depth, m	Grain Density, g/cm <sup>3</sup>	Humidified Drying Effective Porosity, vol%	Convection Drying Effective Porosity, vol%	Increase in Effective Porosity, vol%
1	3293.40	2.7	14.5	14.7	+0.2
2	3294.12	2.7	12.8	13.1	+0.3
3	3295.60	2.7	11.6	11.8	+0.2
4	3296.75	2.7	10.2	10.5	+0.3
6	3298.58	2.7	6.2	6.9	+0.7

water/brine solution is used for both saturation of the sample and measurement of the permeability. A series of pumps or liquid columns is used to flow and measure the solution through the sample while high-accuracy transducers measure differential pressure to determine the permeability of the sample. The test is run at steady state and at multiple conditions to ensure accuracy of the measurements. No slip correction is needed when measuring permeability to water.

### Relative Permeability

Relative permeability testing was conducted on one of the selected core samples and included determination of a drainage curve using supercritical carbon dioxide (CO<sub>2</sub>) and brine. The testing utilized the steady-state method where various ratios of CO<sub>2</sub> and brine were passed through the core until a constant pressure drop was achieved at a known flow rate. The core was held in a Hassler-type core holder at near formation conditions of 81°C and 3000 psia, with a 4000-psia confining pressure. The brine was a synthetic mixture of salts similar to the chemistry of the actual formation brine. Its composition is given in Table A-2. The viscosity of the brine was determined at 81°C using an Ubbelohde viscometer.

A vacuum was pulled on the plug before filling it with brine to assure full initial saturation. The effective permeability to brine ( $K_{ew}$ ) was then determined by forcing the hot brine through the core at a flow rate necessary to create a pressure drop of over 50 psia in order to minimize the capillary end effects inherent in the core. Once  $K_{ew}$  was determined, increasing amounts of supercritical CO<sub>2</sub> were mixed with the brine in order to determine the permeabilities of the fluids relative to  $K_{ew}$  as functions of the brine saturation of the plug. The irreducible brine concentration in the plug was determined by weighing the plug after flowing pure CO<sub>2</sub>. Data from the steady-state testing were then used to construct relative permeability drainage curves for use in the related geophysical modeling efforts.

### X-Ray Diffraction (XRD) Mineralogical Analysis

XRD analysis was conducted to quantify the bulk mineral composition of the samples using the Rietveld refinement method. Standard XRD sample preparation techniques were adopted for these samples, with no major modifications. Rietveld refinements performed were to determine and quantify the crystalline phases; hence, results are reported as relative weight percent of the mineral phases detected.

**Table A-2. Relative Permeability Brine**

Salt	Formula	Concentration, g/L
Barium Chloride	BaCl <sub>2</sub> •2H <sub>2</sub> O	0.067
Strontium Chloride	SrCl <sub>2</sub> •6H <sub>2</sub> O	2.76
Potassium Chloride	KCl	8.35
Magnesium Chloride	MgCl <sub>2</sub> •6H <sub>2</sub> O	13.8
Calcium Chloride	CaCl <sub>2</sub> •2H <sub>2</sub> O	105
Sodium Chloride	NaCl	232

## **Scanning Electron Microscopy**

Thin-section microscope slides used for petrographic optical microscopy analysis were also used for scanning electron microscopy (SEM) analysis. Since the slides were not carbon-coated, the SEM was operated in low-vacuum mode to mitigate charging problems on the samples during analysis. Backscattered electron (BSE) images were obtained on the samples to characterize textural and structural features of the different minerals found in the samples. X-ray signals obtained using the energy-dispersive spectroscopy (EDS) technique were used to identify the chemical composition of the different mineral grains. Finally, the combination of textural and structural features observed from BSE images with the chemical elemental composition obtained from EDS analysis were used to determine the mineral composition of the sample.

Mineral maps, consisting of a composite of several BSE image frames color-coded by mineral phase identified, were also created for the samples analyzed. These maps are used for determining the mineral associations, mineral distributions, 2-D relative area percentages, grain-size visualization, and mineral inclusions of the rock samples.

## **BIBLIOGRAPHY**

- Bush, D.C., and Jenkins, R.E., 1970, Proper hydration of clays for rock property determinations: *Journal of Petroleum Technology*, July 1970, p. 800–804.
- Poppe, L.J., Paskevich, V.F., Hathaway, J.C., and Blackwood, D.S., 2001, A laboratory manual for x-ray powder diffraction: Woods Hole, Massachusetts, U.S. Department of the Interior, U.S. Geological Survey, <http://pubs.usgs.gov/of/2001/of01-041/index.htm>.
- Środoń, J., 1980, Precise identification of illite/smectite interstratifications by x-ray powder diffraction: *Clays and Clay Minerals*, v. 28, p. 401–411.

**APPENDIX B**

**DATA SHEETS**

This page intentionally left blank.